Review

Ice-Templated Method to Promote Electrochemical Energy Storage and Conversion: A Review

Yucheng Wang [1], Yanan Wu [2], Xingqun Zheng [3],*, and Shun Lu [4],*

[1] Cardiff Catalysis Institute, School of Chemistry, Cardiff University, Cardiff CF10 3AT, UK
[2] School of Engineering, Newcastle University, Newcastle Upon Tyne NE1 7RU, UK
[3] College of Safety Engineering, Chongqing University of Science & Technology, Chongqing 401331, China
[4] Chongqing Institute of Green and Intelligent Technology, Chinese Academy of Sciences, Chongqing 400714, China
* Correspondence: zxingqun@cqust.edu.cn (X.Z.); lushun@cigit.ac.cn (S.L.)

Abstract: The ice-templated method (ITM) has drawn significant attention to the improvement of the electrochemical properties of various materials. The ITM approach is relatively straightforward and can produce hierarchically porous structures that exhibit superior performance in mass transfer, and the unique morphology has been shown to significantly enhance electrochemical performance, making it a promising method for energy storage and conversion applications. In this review, we aim to present an overview of the ITM and its applications in the electrochemical energy storage and conversion field. The fundamental principles underlying the ITM will be discussed, as well as the factors that influence the morphology and properties of the resulting structures. We will then proceed to comprehensively explore the applications of ITM in the fabrication of high-performance electrodes for supercapacitors, batteries, and fuel cells. We intend to find the key advances in the use of ITM and evaluate its potential to overcome the existing challenges in the development of efficient energy storage and conversion systems.

1. Introduction

The persistent escalation of the worldwide energy crisis necessitates the advancement and implementation of sustainable renewable energy conversion technologies. Researchers and engineers are currently exploring novel energy resources, with solar and wind energy emerging as the most auspicious sources of renewable energy [1,2]. However, solar energy is constrained by many factors which limit its commercial applications, such as diurnal and seasonal variations, special requirements of geographical location, and other environmental problems. Furthermore, it suffers from relatively low energy flow density, suboptimal efficiency, and high costs [3,4]. Wind energy is facing obstacles such as the variability of wind speed, noise problems, and intermittent power generation. Moreover, effective utilization of wind energy necessitates the integration of energy storage systems to ensure efficient and reliable operation [5]. Compared with wind and solar energy, electrochemical techniques have emerged as promising solutions for energy storage and conversion owing to their several advantages [6–9]. For instance, supercapacitors offer high power density, rapid charge and discharge rates, extended longevity, and secure operation [10–12]. Similarly, fuel cells provide superior energy capacity and higher energy density, coupled with a longer lifespan [13,14]. Electrochemical techniques present a viable means of both storing energy and converting renewable sources of energy, such as solar and wind, into electrical power for storage purposes [15–17]. Despite its advantages, the electrochemical method is beset by certain drawbacks that hinder its widespread adoption, e.g., low reaction activity,

limited lifespan, high costs, and low energy density, which have yet to be adequately addressed [18–20].

In recent decades, researchers have focused on the catalyst and material aspects of electrochemical techniques, while the low mass transfer and charge transfer rates, which hinder the overall energy efficiency, are rarely discussed [8,21]. In conventional 2D electrodes within the electrochemical prototype, the planar current collector has good transfer properties in the 2D plane, and has a limited mass/charge transfer in the depth direction. When using a thicker electrode with a higher mass loading, only a part of the active material is utilized for energy storage due to inadequate charge delivery. Therefore, a 3D electrode structure, such as a 3D conductive scaffold or a 3D porous network, for ion transport can provide efficient charge delivery throughout the bulk volume of a thick electrode. This feature is advantageous for utilizing all electrode materials, regardless of their thickness, and for achieving high-rate and high-capacity energy storage [22].

Here, the ice-templated method (ITM) has drawn significant attention to the improvement of the electrochemical properties of various materials [23], and significant evidence for this can be seen in the increasing number of publications over time, as illustrated in Figure 1. The ITM approach is relatively straightforward and can produce hierarchically porous structures that exhibit superior performance in mass transfer, and the unique morphology has been shown to significantly enhance electrochemical performance, making it a promising method for energy storage and conversion applications [24]. ITM provides several notable advantages over conventional techniques for creating porous structures: (i) it is a green and sustainable process, which employs water ice crystals as a vacancy; (ii) it is a straightforward and easily scalable approach that affords a high degree of control over pore structure; and (iii) it is a cost-effective method that can be adapted to the manufacture of large volumes of materials, rendering it a viable and practical option for industrial applications [25–27].
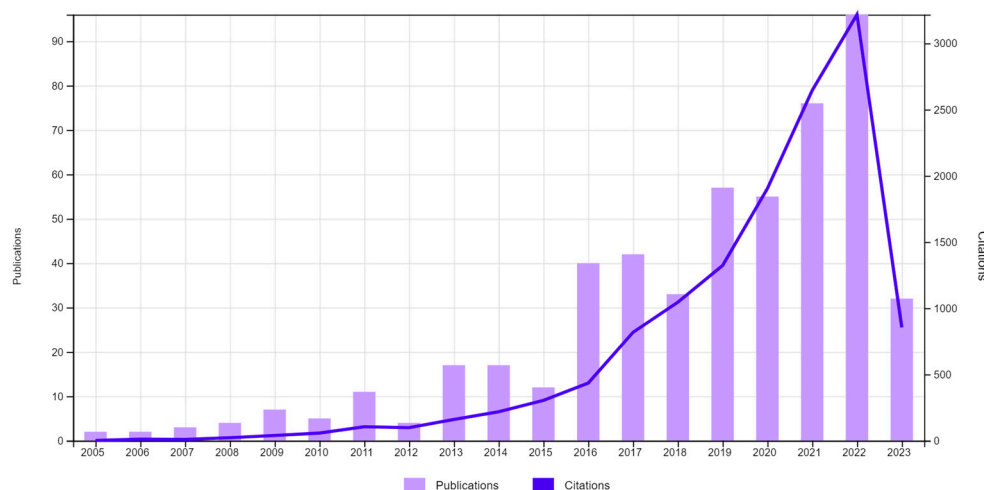

Figure 1. Citation report: ice-templated method (topic) over time, source: web of science.

In this review, we aim to present an overview of the ITM and its applications in the electrochemical energy storage and conversion field. The fundamental principles underlying the ITM will be discussed, as well as the factors that influence the morphology and properties of the resulting structures. We will then proceed to comprehensively explore the applications of ITM in the fabrication of high-performance electrodes for supercapacitors, batteries, and fuel cells. We intend to find the key advances in the use of ITM and evaluate its potential to overcome the existing challenges in the development of efficient energy storage and conversion systems.

2. Methodology of Ice-Templated Method

2.1. ITM Processing Steps

ITM is a technique that utilizes a solvent to induce the formation of a second phase, such as polymers, ceramics, or metals, and promote crystal growth during solidification. The solvent crystals are then eliminated through sublimation, leaving behind a porous structure that mirrors the morphology of the solvent crystals. The microstructure of ice-templated materials is impacted by various factors, including the freezing source and conditions, which significantly influence the structure of the resulting aerogels [28]. The ITM can be classified into different terms, such as freeze drying and freeze casting, and the basic principle of this method is illustrated in Figure 2. The first step is to prepare a suspension of particles in a liquid, which is typically water or a solvent. The second phase is dispersed or dissolved in the solvent. Then the suspension is frozen at a controlled cooling rate, which affects the distribution of the ice crystals that will form during the freezing process. Finally, the frozen material is sublimated to remove the ice from the sample, resulting in a porous, structured material with the particle network preserved.
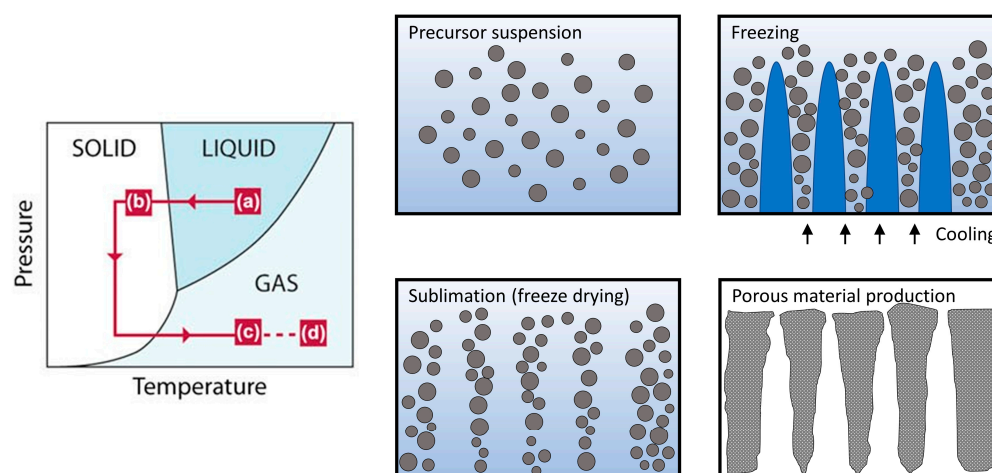
Figure 2. Schematic of the fabrication of porous material by the ice templating method. Reproduced from Ref. [23]. Copyright (2013), with permission from Cambridge University Press.

2.2. Type of Second Phase

The type of second phase (suspended materials) can be varied for multi-applications. It can be, e.g., ceramic [29], which has low thermal conductivity, good corrosion resistance and considerable mechanical strength. Li et al. [30] reported TiN porous ceramics prepared via a freeze-drying and in situ nitridation reaction method using Ti powder and chitosan as raw materials. It showed great potential for use as sulfur host material for lithium–sulfur batteries, with a high capacity of 778 mAh/g. Judez et al. [31] reported a Li-ion conducting glass ceramic (LICGC)-based composite polymer electrolyte (CPE) that delivered high sulfur utilization and areal capacity.

Carbon nano-fibers are considered excellent nano-architectural substrates for supercapacitor applications due to their high power density, good electrochemical cyclic stability, and other desirable properties [28,32,33]. Qie et al. [34] synthesized porous carbon with high-level nitrogen doping using the ITM method as anode material for lithium-ion batteries, producing a reversible capacity of 943 mAh/g at a current density of 2 A/g even after 600 cycles. Wu et al. [35] constructed necklace-box structural FeS_2/WS_2-CNFs, which has resulted in high-performance anodes for LIBs, SIBs, and potassium-ion batteries; moreover, the special spatial confinement structure effectively alleviates volume expansion and protects the carbon shell from being destroyed.

Graphene/GO/reduced graphene oxide (rGO) [36] is regarded as a super lightweight and high conductivity material; it can be used in many applications, such as porous electrodes [30], supercapacitors [37], and sensors [38–40], etc. Chen et al. [41] presented

an ice template method for fabricating flexible macroporous 3D graphene sponges as the anode of microbial fuel cells (MFC), where the graphene sponge was found to be conductive, lightweight, and could recover from deformation repeatedly up to 50%. These sponges generated higher power densities than carbon felt due to their unique porosity, which allows microbes to diffuse more easily inside them, leading better performance. Wang et al. [21] developed a graphene-supported electrode by the ice templating method, and the porous structure enhanced the Faradic efficiency by the promotion of mass transfer.

The metallic particles can be catalytic active sites and capacitors, and ITM treatment provides higher porosity with much lower agglomeration tendencies [34,42]. Li et al. [42] reported that a low-tortuous thick electrode can be successfully designed using a freezing drying route. These types of electrodes have straight lithium-ion transport channels, which allows for independence in electrode thickness and tortuosity. This design accelerates lithium-ion transport and reduces concentration polarization, resulting in excellent rate capability.

Polymer-based porous materials can provide functional groups as reaction active sites, which enhance the electrocatalytic activity and selectivity and offer crucial mechanical stability, flexibility, and durability for electrochemical cells. Colard et al. [43] demonstrated nanoparticle-reinforced soft polymer foams as chemical-sensor components, in which ITM guides and confines the assembly of colloids, resulting in the creation of armored composite self-supporting cellular structures with soft polymer composite matrixes.

2.3. Controlling of Reaction Conditions

ITM is a simple and effective fabrication process performed by adjusting the physical interactions between the suspension and the ice, and also by altering the cooling method of the material in order to control the pore morphologies [44]. The ice crystal growth influences the morphology of the porous structure and depends on the reaction factors below:

Cooling rate: The cooling approach includes unidirectional and multidirectional freezing. In unidirectional freezing, a directional cooling rate will enable a temperature gradient in solution, which causes ice to grow towards the applied field. The growing ice front displaces particles via diffusion and convection, accumulating them at the ice/liquid boundary layer. Arabi et al. [45] reported the effect of cooling rate influence on ice templating of gelation scaffolds; by increasing the cooling rate, the average pore size decrease, and there is no apparent difference between the morphology of pores. This is because a higher cooling rate results in smaller nuclei of ice crystals, which are, therefore, smaller in size. At a lower cooling rate, water molecules have enough time for nucleation and growth. Figure 3a–f show the cooling rate influence of the gelatin scaffolds. Meanwhile, the compressive strength increases by increasing the cooling rate, as shown in Figure 3h. In multidirectional solidification with low external temperature gradients, equiaxial growth is observed throughout the sample, resulting in isotropic pore distribution in the scaffolds.

Concentration of solution/suspension: the concentration of particles in the suspension can affect the porous morphology and structure. The porosity value of the material can be calculated according to Equation (1).

$$\text{Porosity} = (V_m - (W_m/\rho))/V_m \times 100\% \tag{1}$$

where V_m is the volume of solution/suspension (cm^3), W_m is the mass of the scaffold (g), and ρ is the density of the gelatin. Hence, high concentrations of solution/suspension will reduce the porosity of the material. As shown in Figure 3i–n, the pores in lower-gelatin concentrations appeared oblate and polygonal in shape, and by increasing the concentration, the pores became more circular. Additionally, increasing the gelatin concentration resulted in a reduction in pore channel size and layer distance. This may be attributed to the increase in solution viscosity with increasing gelatin concentration, which required a higher force for gelatin molecules to be expelled by water molecules. As a result, smaller ice crystals were formed, leading to smaller pore sizes.
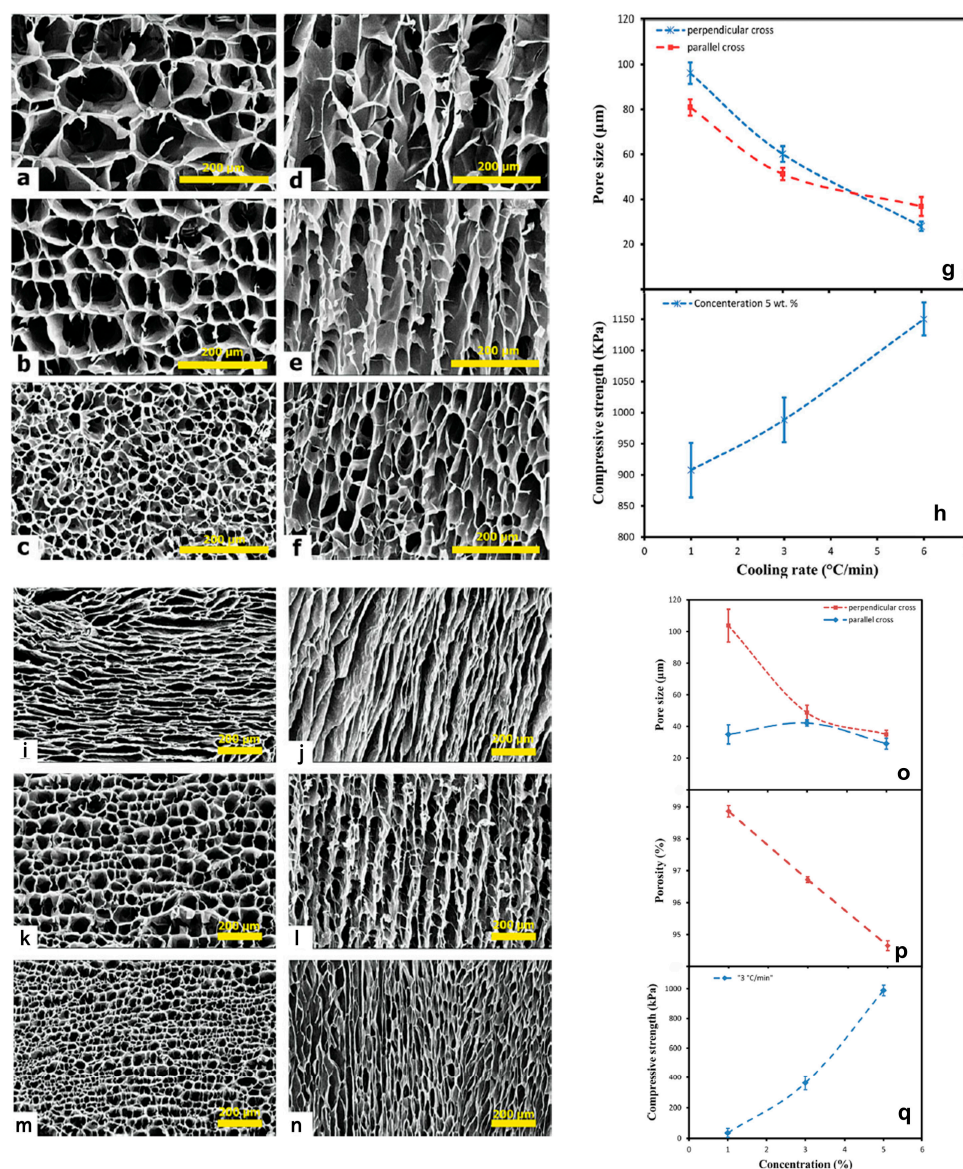
Figure 3. SEM images of 5 wt% gelatin scaffolds with cooling rate of (**a**,**d**) 1 °C/min, (**b**,**e**) 3 °C/min, and (**c**,**f**) 6 °C/min. (**g**,**h**) Compressive strength and pore size distribution of 5 wt% gelatin scaffolds at various cooling rates. SEM image of gelation with cooling rate of 3 °C/min (**i**,**j**) 1 wt% (**k**,**l**) 3 wt%, and (**m**,**n**) 5% wt&. The direction of the cross-section is perpendicular and parallel to the ice growth front. (**o**–**q**) Effect of gelatin concentration on the compressive strength, total porosity, and pore size of scaffolds with a rate of 3 °C/min. Reproduced from Ref. [45]. Copyright (2013), with permission from Wiley-VCH.

For electrochemistry applications, controlling the ITM is advantageous since it has a substantial impact on the electrochemical characteristics, such as surface area, porosity, and catalytic activity. For electrochemical reactions, for instance, a porous shape might offer high surface reaction active area, whereas a hierarchical structure can improve mass transport and catalytic activity. Controlling the morphology can also increase the material's stability and toughness, making it better suited for long-term electrochemical applications. To create high-performance electrochemical devices, such as batteries, fuel cells, and sensors, morphology control of porous materials using the ITM approach is the key part.

3. Applications in Electrochemistry for Energy Storage

Porous materials have garnered significant attention in the field of electrochemistry for energy storage applications due to their unique properties such as high surface area and high porosity [46]. The ability to control the pore size distribution, morphology, electrical, and physical properties of porous materials is a critical aspect in their manufacturing. In this regard, the ITM method has emerged as an effective technique for precisely controlling the characteristics of porous materials.

The ITM method has become a crucial tool for the fabrication of porous materials for energy storage applications. For instance, porous carbon materials, such as activated carbon, carbon aerogels, and carbon nanotubes, are widely used as electrode materials due to their high surface area and excellent electrical conductivity in supercapacitors; these materials can store charge by adsorbing ions on their surface or within their pores, which enables them to achieve high energy and power densities [47–49]. In fuel cells and electrochemical reactors, porous materials can be used for the manufacturing of electrodes, including making porous catalyst layers, gas diffusion layers, and ion exchange membranes [50–52]. The mass transfer and charge transfer can be optimized by controlling the the porous material using ITM, which reduced the internal resistance within the reactor and results in high Faradaic efficiency and energy efficiency. The application of ITM in electrochemistry will be discussed separately according to different field.

3.1. Supercapacitors

Supercapacitors are devices which provide high power rates compared to batteries. They are capable of much higher power in the same volume as batteries, but with 3–30 times lower energy storage. This makes them well-suited for applications where short bursts of power are needed but high energy storage capacity is not necessary [53].

As shown in Figure 4, in designing of supercapacitors, ITM can creating well-controlled porous structures in the materials used for the electrodes. Porous structures with high surface area can provide more space for energy storage and improve the performance of supercapacitors. By tuning the volume of the ice template used in this process, it is possible to control the size and shape of the hollow cavities formed in the inner space of the porous material. This can enlarge the accessible surface area and expose extra ion storing sites. The increased surface area provided by these porous structures can improve the performance of supercapacitors by providing more space for energy storage. Additionally, having more ion storing sites can shorten the ion diffusion distance and further improve the performance.
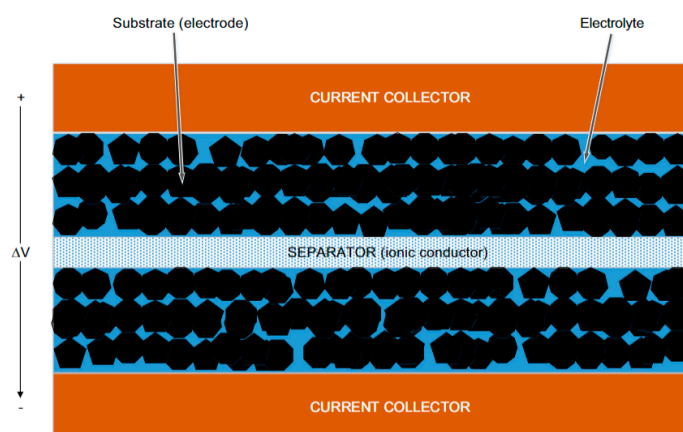

Figure 4. Symmetric supercapacitor schematic diagram. Reproduced from Ref. [53]. Copyright (2016), with permission from Elsevier.

3.1.1. Carbon-Based Materials as Electrodes

Carbon-based materials, especially graphene, show low density, high specific surface area, good conductivity, and mechanical stability. In recent years, there has been

a growing research interest due to its potential for a variety of applications, including as electrodes in supercapacitors [54,55]. There have been several reported methods for preparing carbon/graphene/reduced graphene oxide (rGO) aerogels.

Thomas et al. [28] discussed the properties and potential applications of carbon aerogels, which are materials with a 3D hierarchical network structure and high specific surface area. This paper introduces a new, green, and facile preparation route involving ice-templating and lyophilization followed by carbonization for the preparation of carbon aerogels, as shown in Figure 5. We investigated the effects of different factors on the structure and electrochemical performance of the resulting aerogels, and demonstrated the superior electrochemical performance of the prepared aerogel electrodes. By controlling the cooling rate and the concentration of solid content of lignin and cellulose nanofibers, this work achieved the highest surface area of 1260 m^2/g and an excellent specific capacitance of 410 F/g at 2 mV/s. This method also has good cyclic stability of the electrodes, which, after 4500 charge-discharge cycles, was 94%.
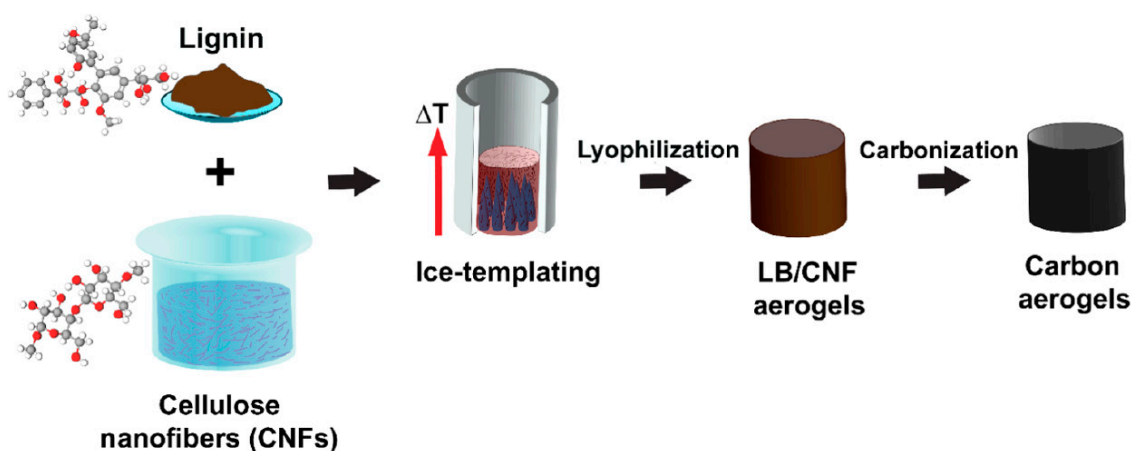

Figure 5. Schematic representation of various processes involved in the preparation of Cas. Reproduced from Ref. [28]. Copyright (2022), with permission from the American Chemical Society.

Compared with carbon, graphene forms a unique 2-dimensional honeycomb crystal structure, which provides a good pathway for electron transfer and also benefits the physical and chemical properties [56]. Ni et al. [57] reported a hierarchically multi-layered porous carbon (HPC) successfully prepared using ITM (Figure 6), The graphene content was found to have a significant impact on the structure of the HPC. The resulting HPC exhibited a high surface area of 2078.4 $m^2 \, g^{-1}$ and showed good electrochemical properties in different electrolytes. The HPC also displayed a specific capacitance of 201 F/g at a current density of 0.5 A/g and excellent cycling performance of 103% initial capacity retained after 10,000 cycles at 10 A/g. The supercapacitor also showed excellent cycling performance, with 94.4% capacitance retention after 5000 cycles. Similarly, Mochizuki et al. [58] developed porous electrodes with nanosheets vertically aligned to the substrate (Figure 7). The process of producing rGO films, which are vertically aligned, involves combining the electrophoretic deposition technique with the ice template method. The perpendicular orientation of graphene oxide with respect to the substrate enhances the specific capacitance and charging rate behavior. The specific capacitance was approximately 78% of that at 2 mV/s at a high scan rate of 500 mV/s, indicating an improvement in the rate performance by controlling the film thickness and pore sizes.
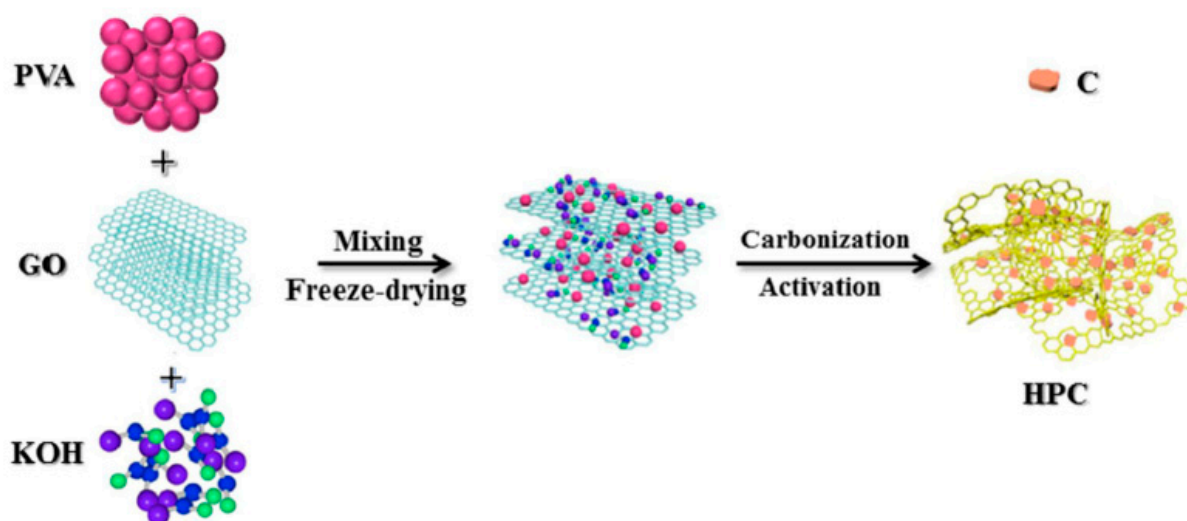
Figure 6. Schematic diagram for the preparation of HPC. Reproduced from Ref. [57]. Copyright (2021), with permission from Springer.
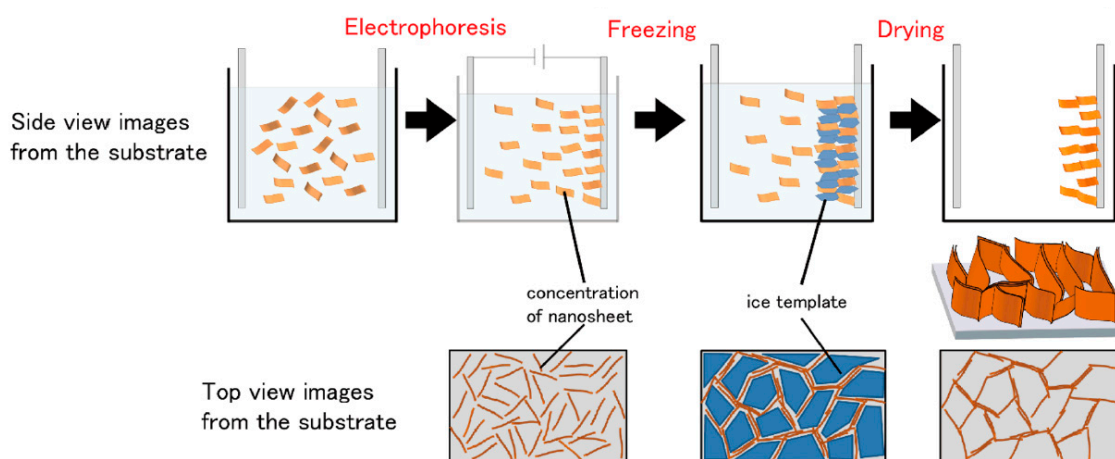

Figure 7. Proposed formation mechanism of the vertically aligned film by electrophoresis and freeze drying. Reproduced from Ref. [58]. Copyright (2019), with permission from the American Chemical Society.

However, graphene can be prone to aggregation, which can reduce its overall surface area and therefore its capacitance [59]. This problem can be mitigated using appropriate surface functionalization and stabilization techniques, such as nitrogen doping into the graphene lattice, which can alter the electronic structure of the material, leading to enhanced electrical conductivity. Kota et al. [60] reported a 3D macro-porous nitrogen-doped graphene using an ice-templating method (Figure 8). Such a method produces unique properties of Ni-doped graphene, including a hierarchal porous structure and uniformly distributed nitrogen atoms, which enhance its electrochemical performance as a supercapacitor electrode material. The nitrogen doping in the honeycomb lattice provides noticeable pseudocapacitive behavior along with electric double layer capacitor formation, and the pyridinic-type nitrogen configuration provides excellent electrochemical stability due to the higher charge density.
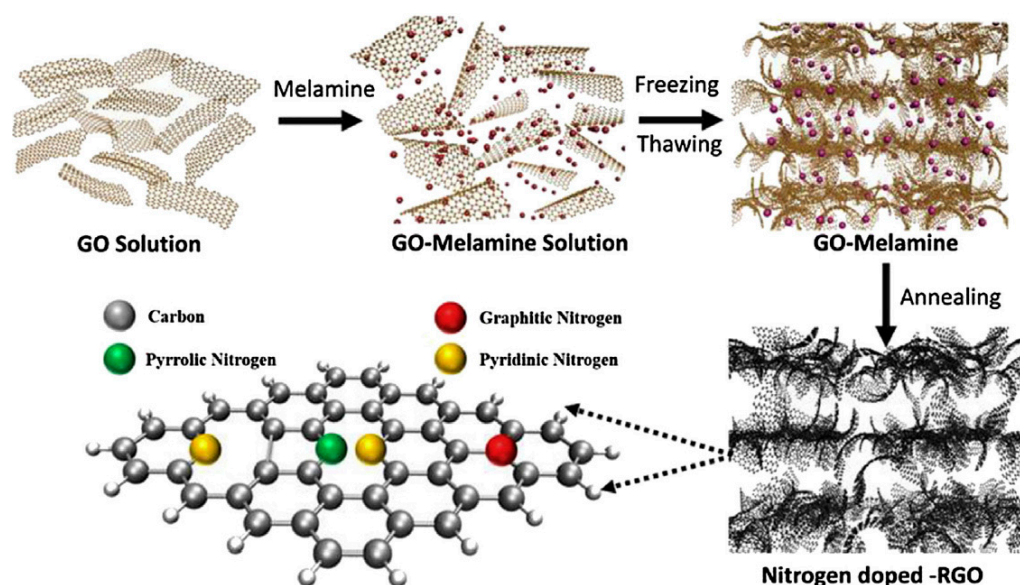
Figure 8. Synthetic procedure for synthesis of N-doped graphene and different N-doped configurations in the graphene lattice. Reproduced from Ref. [60]. Copyright (2016), with permission from Elsevier.

Deng et al. [60] discussed the current challenges in creating flexible supercapacitor devices for wearable technology, and this research proposes a novel fabrication strategy for creating a flexible and high energy density supercapacitor device by combining nickel foam and pseudocapacitive nickel oxide via oriented graphene oxide filling. Here, the ITM method is applied to fill the nickel foam with oriented graphene oxide aerogel. The device exhibits excellent flexibility and is capable of achieving a high electrochemical capacitance. The activation process occurs during both electrochemical and deformation cycles, leading to a remarkable 102% retention of capacitance after 500 repeated deformations and 80% retention after 3000 charge/discharge cycles. The areal capacitance reaches a record high of 479.8 mF/cm^2, while the energy density and power density reach up to 1.69 Wh/m^2 and 9 W/m^2, respectively.

3.1.2. MXene as Electrodes

MXenes have shown potential in energy applications in batteries and supercapacitors due to their 2D layered structure and good conductivity, hydrophilicity, and chemical stability [61]. However, they still face challenges, such as restacking and aggregation of nanosheets, which can result in poor electrochemical properties [62]; the electrodes have a limited surface area face to the electrolytes, and this results in low gravimetric capacitance. One of the strategies is to assemble the 2D MXene into a 3D porous material as an electrode using ITM; this method offers precise control over the size and shape of the resulting carbon structure, as well as the pore size distribution and surface area. The porous structure provides a pathway for ionic transfer and avoids the agglomeration problem, therefore enhancing the stability of the supercapacitor. For MXene application in supercapacitors using ITM, Gao et al. [63] reported a dual-step strategy for the 3D porous MXene fabrication (Figure 9). A 3D porous MXene with a homogeneous layered structure and large interlayer spacing was assembled through two distinct steps: the first step involved controlling the nucleation during freezing by adjusting the temperatures and cooling rates, while the second step involved the expansion of layers during freezing, which is growth-dominant freezing. The porous structure of the electrode increases the surface area and enhances ion transport, leading to higher specific capacitance and better cycling stability. Similarly, Cai et al. [64] reported a super elastic MXene aerogel with outstanding electrochemical properties, high-rate capacity, and temperature-invariant super-elasticity, making them suitable for use in supercapacitors and wearable electronic devices (Figure 10).

The assembled symmetric MXene supercapacitors showed an excellent energy density of 38.5 μWh/cm^2 and an excellent cycle stability of 86.7% (after 4000 cycles), as well as excellent photo-response ability.
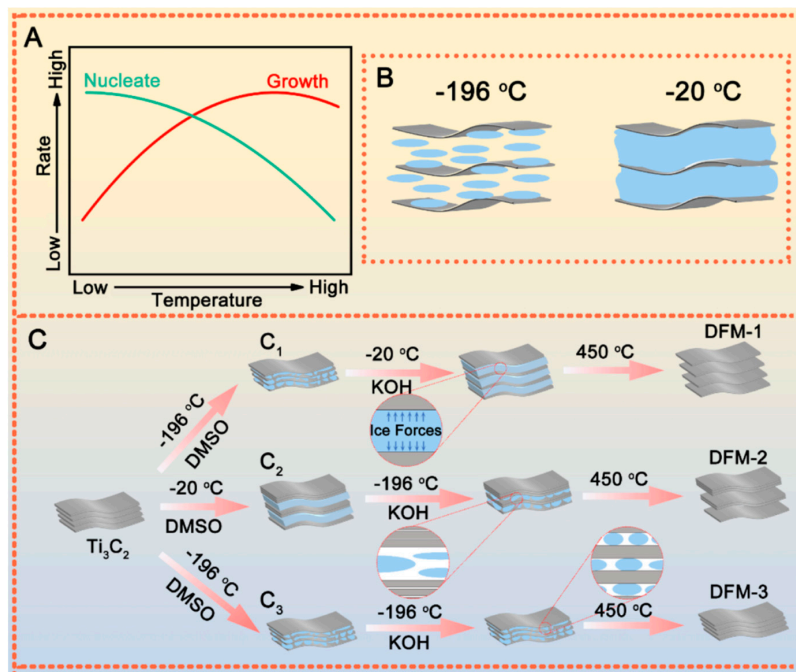

Figure 9. (**A**) The ice crystal formation kinetics with the change of temperature and cooling rate. (**B**) The schematic of ice crystals within MXene interlayers under different temperatures. (**C**) The illustration of dual-step freezing protocols for the synthesis of MXenes with different conditions. Reproduced from Ref. [63]. Copyright (2022), with permission from Elsevier.
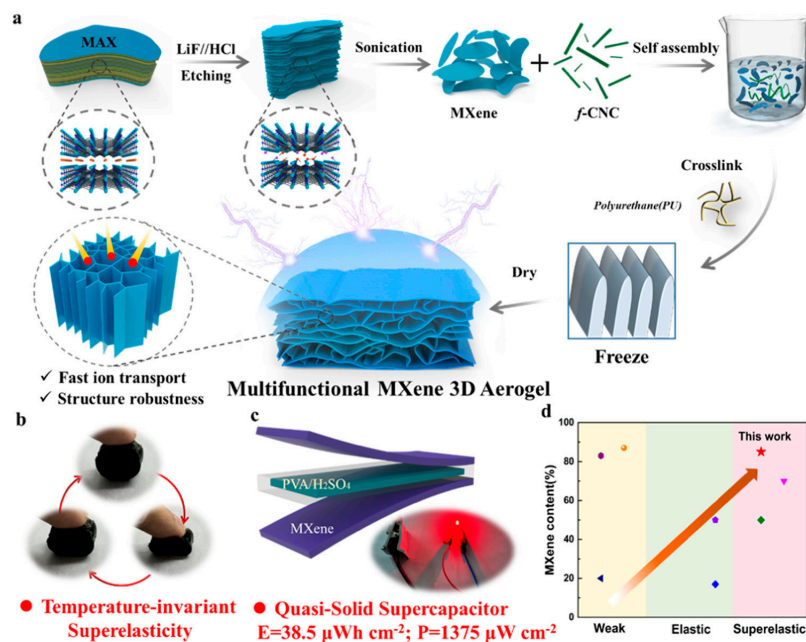

Figure 10. Strategy for constructing MXene 3D-aerogel via cryo-assembly: (**a**) Preparation process of MXene aerogels; (**b**) Temperature-invariant superelasticity property of MXene aerogels; (**c**) Assembled MXene-based supercapacitor; and (**d**) Curve of mechanical property vs. MXene loading. Reproduced from Ref. [64]. Copyright (2021), with permission from the American Chemical Society.

Compared with pure MXene as a material for a 3D porous structure, Zhang and colleagues successfully produced a flexible, free-standing 3D porous film (3D-PMCF) composed of MXene and carbon nanotubes using a freeze-drying technique. The incorporation of CNTs in the hydro-film has been found to increase the amount of interlayer water and the resulting porosity [65]. The 3D structure of MXene significantly enhances the number of exposed surface-active sites and promotes ion transport while maintaining flexibility. The 3D-PMCF film exhibits a capacitance of 375 F/g at 5 mV/s and retains 251.2 F/g at 1000 mV/s with excellent cycling stability, which is significantly better than the conventional $Ti_3C_2T_x$ film with densely stacked structures. The assembly of the 3D-PMCF film into a symmetric supercapacitor has yielded an energy density of 9.2 Wh/kg. Figure 11 shows the synthesis process of the 3D porous MXene/CNTs film electrode. The process involves the preparation of a hydro-film of MXene/CNTs by vacuum-assisted filtration of a MXene/CNTs suspension.
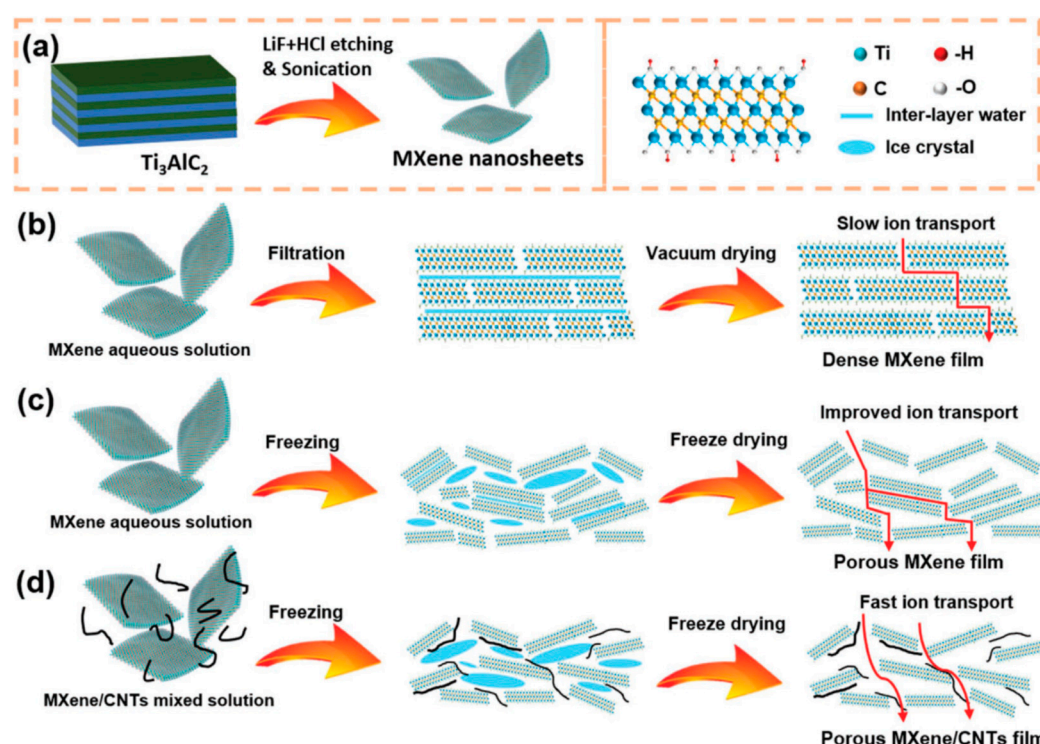

Figure 11. Schematic illustration of the fabrication process of (**a**) MXene nanosheets, (**b**) vacuum-dried D-MF film, (**c**) freeze-dried 3D-PMF film, and (**d**) freeze-dried 3D-PMCF film. Reproduced from Ref. [65]. Copyright (2020), with permission from Wiley.

3.1.3. Polymer-Based Supercapacitors

Polymer-based ionic conducting gels are becoming popular electrolyte materials for soft supercapacitors due to their flexibility, wearability, and portability with minimal liquid leakage [66]. Hydrogels with highly ordered 3D structures also exhibit desirable anisotropic properties, such as enhanced directional ion transfer. Among these approaches, ITM is a promising and versatile method for creating well-defined polymer-based porous materials. For example, Zhao et al. [67] reported a novel approach to creating a flexible all-solid-state hydrogel supercapacitor, which was inspired by wood. Figure 12 illustrates the ice-templating process used to create the aligned hydrogel matrix. By modifying the morphology of the hydrogel matrix, it becomes possible to increase the electrode material loading and areal capacitance. This is accomplished through the alignment of the matrix, resulting in enhanced morphological flexibility, exceptional mechanical flexibility, and uniform polypyrrole distribution, even in matrices up to 7 mm thick. The supercapacitor demonstrates impressive performance metrics, including a high energy

density of 73.8 μWh/cm^2, a power density of 4960 μW /cm^2, an 86.5% capacitance retention after 1000 cycles, and a 95% bending stability after 5000 cycles.
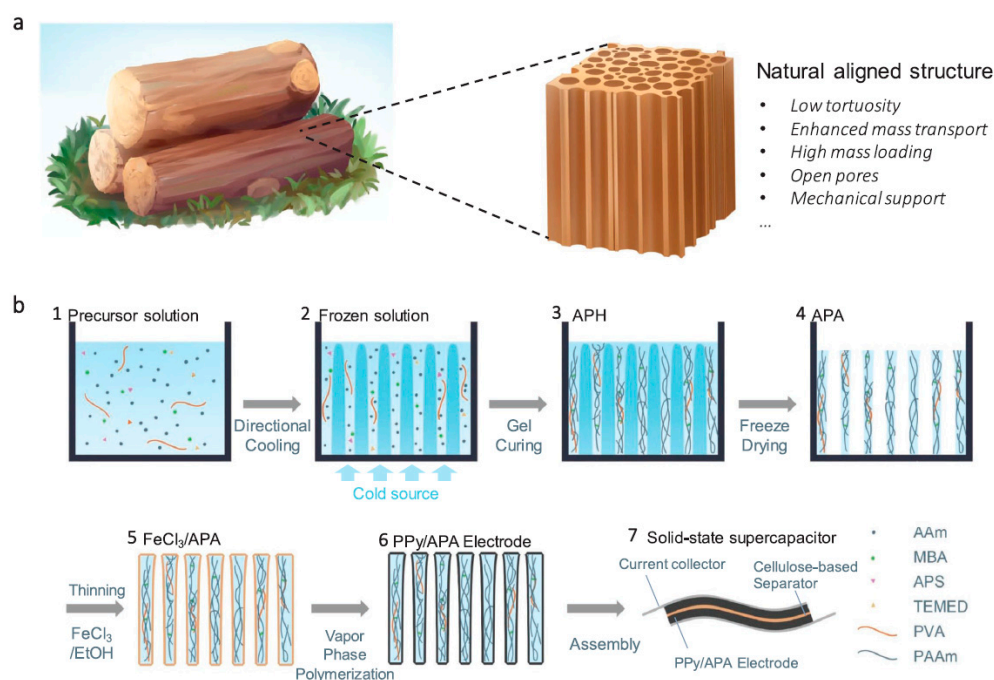

Figure 12. Schematic of the fabrication of all-solid-state hydrogel supercapacitors via integration of APA as the matrix and PPy as the electrode material. Reproduced from Ref. [67]. Copyright (2020), with permission from Wiley.

Similarly, Wei et al. [68] used polyampholyte-doped aligned polymer hydrogels as anisotropic electrolytes for supercapacitor applications. The paper focuses on the pressure-resistant polymer gel electrolytes with ion channels for wearable energy devices. They used a biomimetic aligned hierarchical design and polyampholyte doping to achieve high strength and large ionic mobility. The preparation of hydrogel is shown in Figure 13. The monomers were polymerized around the ice, and the aligned porous structure hydrogel was obtained after the removal of crystals. For the results, the authors found that the optimized supercapacitor capacity of the aligned gel electrolytes was higher than that of a liquid electrolyte. By optimizing the supercapacitor with the aligned gel electrolytes, the capacity achieved 201.5 F/g at a 0.1 A/g current density in the vertical direction, which is higher than the liquid electrolyte's capacity of 159.0 F/g.

Liu et al. [69] developed high-temperature supercapacitors using aligned ionogel electrolytes, which was achieved by ITM. The aligned ionogel electrolytes can significantly improve the performance of high-temperature supercapacitors. This novel design can consistently achieve superior electrochemical performances at all temperatures relative to the nonaligned device, with a 29% higher specific capacitance (176 F/g at 25 °C and 1 A/g). Moreover, under high temperatures of 200 °C, the thermally stable aligned ionogel has a high ionic conductivity of 22.1 mS/cm and with a high specific capacitance of 167 F/g at 10 A/g (Figure 14). It has the potential to be used in the development of high-temperature supercapacitors for various applications.
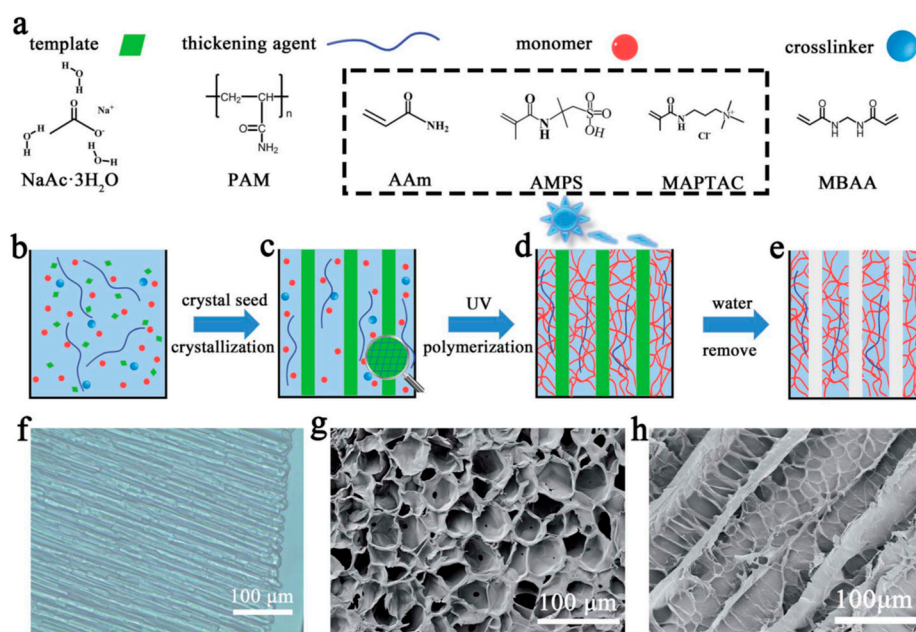
Figure 13. Schematic showing the preparation of hydrogels with an aligned porous structure by the "hot ice" template method. Reproduced from Ref. [68]. Copyright (2018), with permission from the Royal Society of Chemistry.
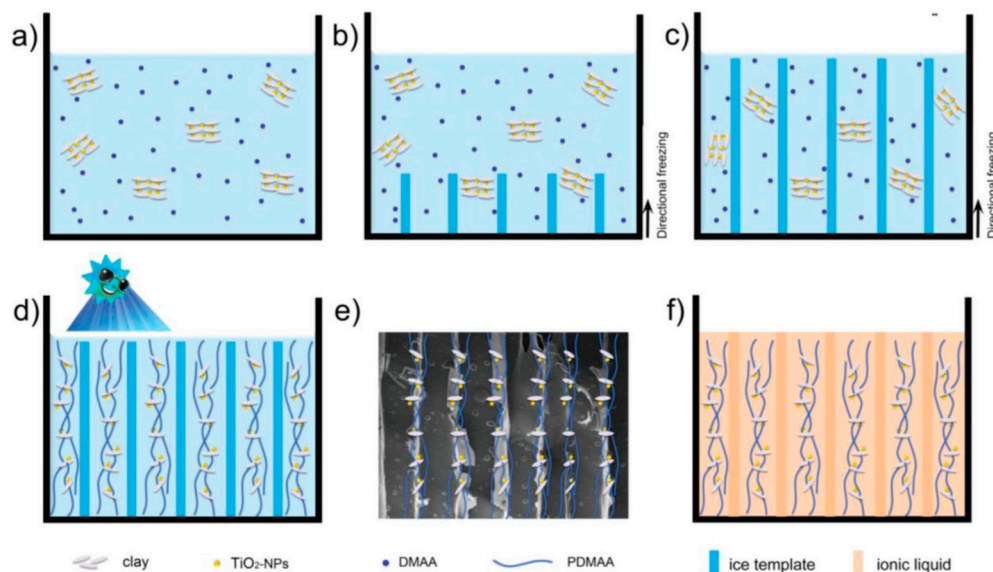

Figure 14. Proposed schematic illustration of the preparation of an aligned hydrogel by applying a directional freezing process (**a**) The precursor aqueous solution of clay-Ns, DMAA, and TiO$_2$-NP in water. (**b**,**c**) The monomer-nanoparticle composite is excluded from the directionally freezing of the orientated ice crystals. (**d**) The monomer is cryopolymerized to produce hydrogel with an aligned structure. (**e**) SEM image of the freeze-dried polymer matrix with aligned structure. (**f**) The aligned ionogel can be obtained by adding ionic liquid to freeze-dried aligned polymer matrix. Reproduced from Ref. [69]. Copyright (2019), with permission from Wiley.

3.2. Li Ion Batteries (LIBs)

Compared to other energy storage systems for stationary power storage, rechargeable LIBs have gained significant attention due to their high energy densities, non-memory effect, environmentally friendly technology, and long cycle life [70]. However, despite their many advantages, thick electrodes in the battery pose a challenge, as they restrict

lithium-ion transport kinetics due to prolonged diffusion lengths and tortuous transport pathways [71]. It is worth noting that the use of porous electrode materials, particularly mesoporous ones, may significantly improve the power rate during the electrochemical process by providing a large surface area and abundant migration channels which can accelerate ion migration at the electrolyte–electrode interface. Therefore, the ITM strategy is a cost-effective, environmentally friendly, and versatile approach for creating aligned porous electrodes in LIBs. It allows for sophisticated and precise control over electrode materials, resulting in uniquely structured morphologies. Figure 15 shows the sketch of the LIBs, and we classified it into three parts, according to the ITM application: cathode, anode, and solid electrolyte.
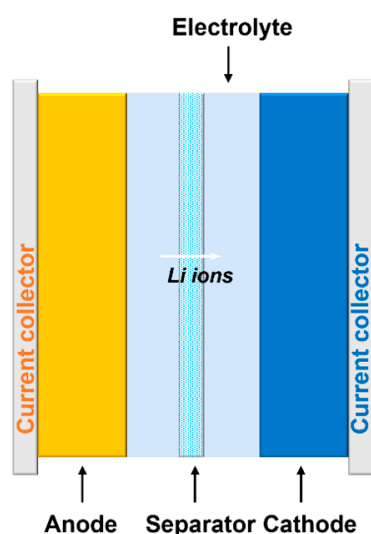

Figure 15. Sketch of LIBs.

3.2.1. Cathode Material in LIBs

The majority of research in the field has focused on enhancing the high specific surface area and Li ion transfer of thick cathode materials. One approach to achieve this is by employing ice as a template to regulate the material's morphology and create an abundance of porous channels. This technique has been successfully applied to a variety of lithium-ion batteries, such as lithium–cobalt oxide batteries, lithium–manganese oxide batteries, and lithium–iron phosphate batteries.

For lithium–cobalt oxide batteries, Huang et al. [72] reported an ultra-thick $LiCoO_2$ (LCO) cathode (Figure 16) for lithium-ion batteries using the ITM method, which builds a gradient of pore structures throughout the electrode thickness to enhance energy densities at fast rates. The resulting electrodes have demonstrated significantly higher gravimetric energy density at the cell-stack level, compared to conventional electrodes with random structures and identical materials. The superior performance of the ice-templated electrodes is attributed to several factors, including the improved uniformity of ion mobility throughout the thick electrode; the low electrical resistance of the oriented struts of well-packed primary active materials with a large, exposed electrolyte/LFP contact area; and a substantially reduced proportion of inactive components at the cell-stack level. These findings are detailed in Figure 16. The ice-templated electrodes exhibit a capacity of 94 mAh/g at an ultra-high current density of 15 mA/cm^2, while conventional electrodes exhibit only 47 mAh/g.
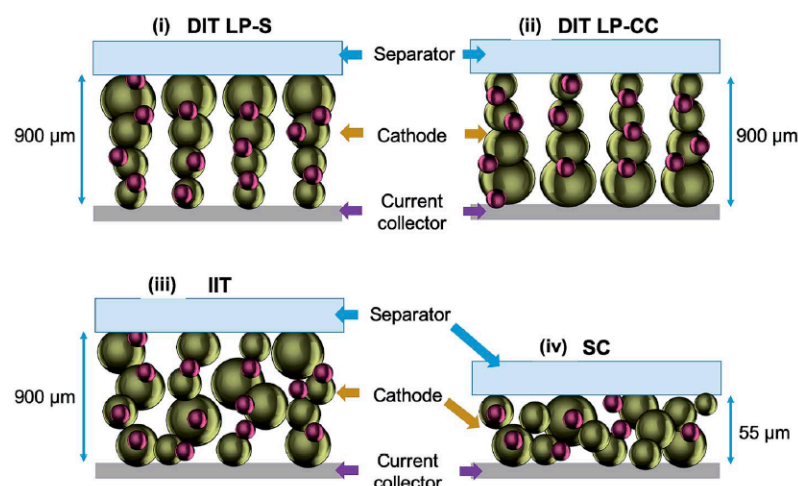
Figure 16. Schematics of the four electrode types fabricated for performance comparison. Reproduced from Ref. [72]. Copyright (2019), with permission from the Royal Society of Chemistry.

Li et al. [72] reported a hierarchical mesoporous Li[Li$_{0.2}$Ni$_{0.2}$Mn$_{0.6}$]O$_2$ microsphere composed of nanoparticles synthesized using ITM combined with a coprecipitation strategy, as demonstrated in Figure 17. The results indicated that the electrochemical performance of the sample prepared using the ITM was superior to that prepared using the conventional coprecipitation method. The former exhibited enhanced capacity, improved cycling stability, and superior rate capability. These enhancements were attributed to the stable hierarchical micro-sized structure and the improved lithium-ion diffusion kinetics resulting from the highly porous structure. The ice-templated electrode showed satisfactory initial discharge capacities of 280.1 mAh/g at 0.1 C, 207.1 mAh/g at 2 C, and 152.4 mAh/g at 5 C, along with good cycle performance.
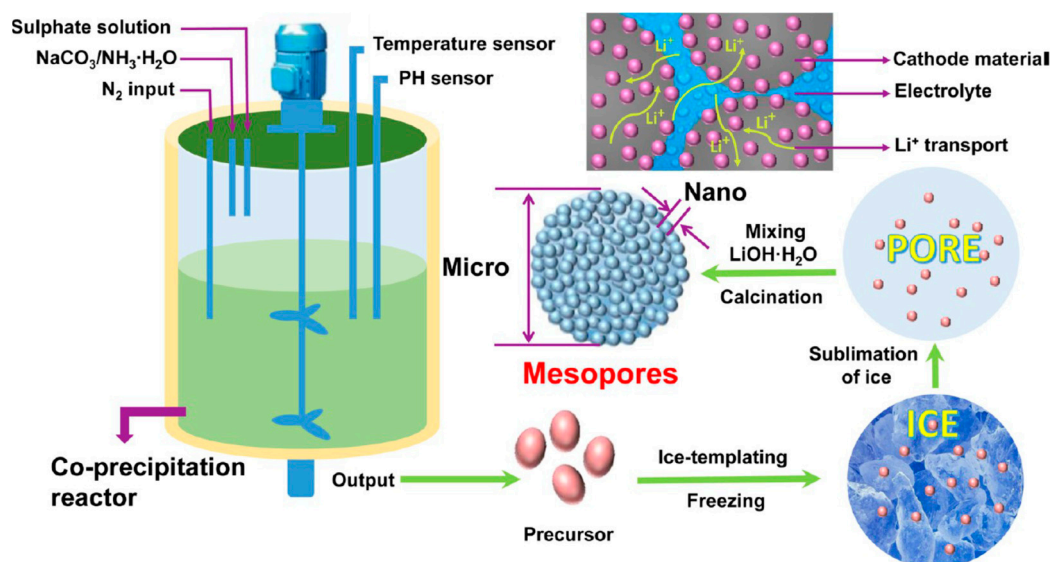

Figure 17. Schematic diagram of the synthetic route for hierarchical mesoporous cathode material Li[Li$_{0.2}$Ni$_{0.2}$Mn$_{0.6}$]O$_2$. Reproduced from Ref. [72]. Copyright (2020), with permission from the American Chemical Society.

Li et.al. [42] developed an ultrathick and low-tortuous LiFePO$_4$ electrode using ITM (Figure 18). The low-tortuosity design of the electrodes provides straight pathways for lithium-ion transport, resulting in enhanced transport and reduced concentration polarization, thereby improving their rate capability. Meanwhile, the low-tortuous thick electrodes display a uniform and highly reversible electrochemical reaction, promoting superior

cyclability. The study demonstrated that the FDLFP electrode, with a mass loading of 22.30 mg/cm^2, delivered a specific capacity of 151.4 mAh/g at 1 mA/cm^2 for 200 cycles.
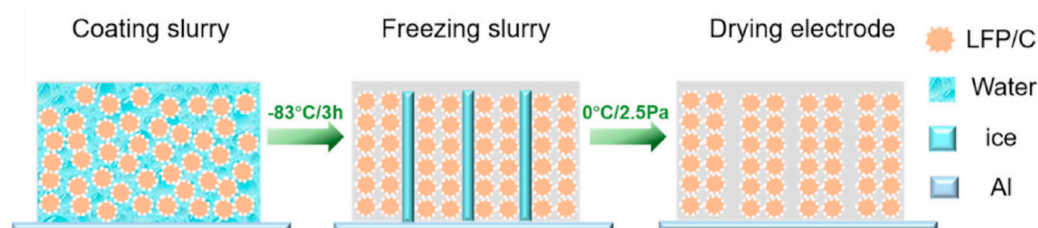

Figure 18. Schematic diagram of freezing dry method of the LiFePO$_4$ electrode. Reproduced from Ref. [42]. Copyright (2020), with permission from Elsevier.

3.2.2. Anode Material in LIBs

Porous material can not only be applied on cathodes in LIBs, but also on anodes to achieve higher capacities and power densities. For instance, carbon based materials are commonly used as material on anodes. Roberts et al. [73] found that, when applying 3D porous carbon structures using ITM, it shows superior anode performance compared to other forms of carbon, particularly in terms of specific capacity and high-rate performance. In this work, Robert prepared hierarchically porous carbon monoliths from a polyacrylonitrile (PAN) precursor using a simple ITM (Figure 19). The carbon monoliths possess a naturally high nitrogen content and exhibit good capabilities in terms of specific capacity and high-rate performance as anode materials in lithium-ion batteries. This enhanced performance is ascribed to the hierarchical pore structure, which facilitates the efficient transport of lithium ions, as well as the nitrogen-rich precursor and self-doping mechanism employed to achieve an exceptionally high nitrogen content.
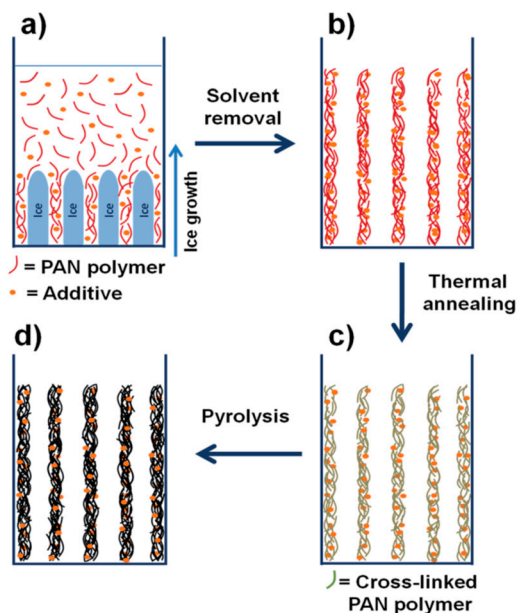

Figure 19. Schematic representation of the process in which the ice templated PAN-derived porous carbons are created. Reproduced from Ref. [73]. Copyright (2014), with permission from the Royal Society of Chemistry.

In a study by Wang and colleagues, a hybrid nanoarchitecture aerogel composed of WS$_2$ nanosheets and carbon nanotube–reduced graphene oxide (CNT-rGO) was synthesized to serve as an anode material for both lithium- and sodium-ion batteries (LIBs and SIBs) [36]. The aerogel structure featured an ordered 3D scaffold microchannel, which facilitated efficient electronic and ionic conductivity and resulted in enhanced electrochemical

performance. The WS_2/CNT-rGO aerogel nanostructure exhibited a specific capacity of 749 mAh/g at 100 mA/g and a high first-cycle coulombic efficiency of 53.4% as the anode material of LIBs. Additionally, it delivered a capacity of 311.4 mAh/g at 100 mA/g and retained a capacity of 252.9 mAh/g at 200 mA/g after 100 cycles of SIBs. The excellent electrochemical performance was attributed to the synergistic effect between the WS_2 nanosheets and the CNT-rGO scaffold network, as well as to the rational design of the 3D ordered structure, as illustrated in Figure 20.
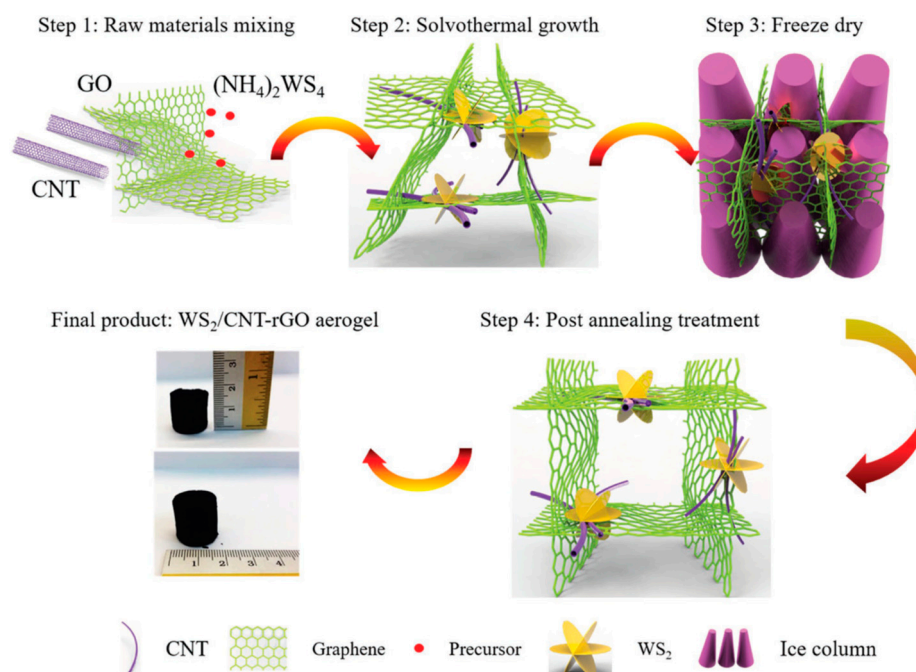

Figure 20. Schematic diagram of WS_2/CNT-rGO aerogel 3D ordered microchannel nanoarchitecture synthesis process. Reproduced from Ref. [36]. Copyright (2016), with permission from Wiley.

3.2.3. Electrolyte Material in LIBs

Interestingly, some of the research focuses on the composite solid electrolytes within the Li/Li-ion batteries in order to increase the ionic conductivity. The ITM can be used to build a vertically aligned porous ceramic/polymer composite electrolyte in rechargeable solid-state Li-/Li-ion batteries. Zhai et al. [74] reported a composite electrolyte using a polymer matrix with ceramic Li-ion conductors dispersed inside (Figure 21). ITM was used to fabricate the vertically aligned and connected $Li_{1+x}Al_xTi_{2-x}(PO_4)_3$ nanoparticles (LATPNPs) in the poly(ethylene oxide) (PEO) matrix to maximize the ionic conduction and provide good flexibility of the composite. This design shows a conductivity of 0.52×10^{-4} S/cm, which is 3.6 times that of the composite electrolyte with randomly dispersed LATPNPs.

3.3. Fuel Cell Type Electrochemical Reactor

The design of novel porous electrode architecture and the study of mass/ion transfer within the structures are the core issues in developing fuel cells and other electrochemical energy electrolysers [75]. Currently, electrochemical reactors suffer from gas diffusion through the electrode, insufficient ion transfer within the electrolyte/flow channel, or difficult electron transfer between the gas diffusion layer and catalyst layer [50]. One of the solutions is to use porous material as electrodes, or to replace the flow channels for better mass/ion transfer. ITM is a promising method for delivering well-defined macro-pore structures, and it can further enhance the energy efficiency and reaction rate by promoting the mass/ion/charge transfer.
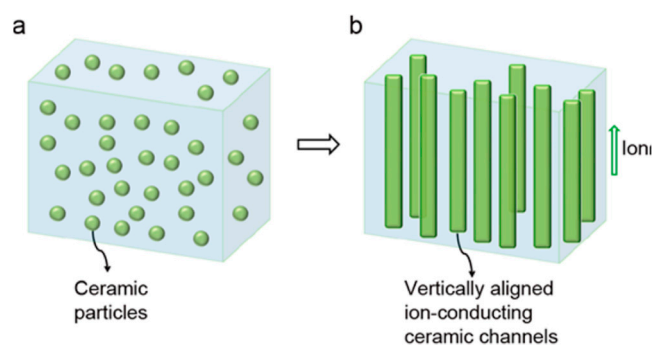
Figure 21. Schematic of vertically aligned and connected ceramic channels for enhancing ionic conduction. (**a**) Ceramic particles are randomly dispersed in the polymer matrix, where ion transport is blocked by the polymer matrix with a low conductivity. (**b**) Vertically aligned and connected structure to facilitate ion transport, which can be realized by the ice-templating method Reproduced from Ref. [74]. Copyright (2017), with permission from the American Chemical Society.

Xia et al. [66] reported an ITM application on direct methanol fuel cells. The macro-porous structure enhances mass transport and boosts electrochemical properties, resulting in a remarkable improvement in energy production and in the efficiency of direct methanol fuel cells with 73% for peak power density. Wang et al. [21] designed a porous graphene aerogel using the ITM method, and applied it as an electrode in an electrochemical CO_2 reduction reaction reactor. The porous design benefits CO_2 mass transfer and provides a pathway for charge transfer. The advanced design increases the Faraday efficiency to over 94% toward CO and formate (Figure 22).
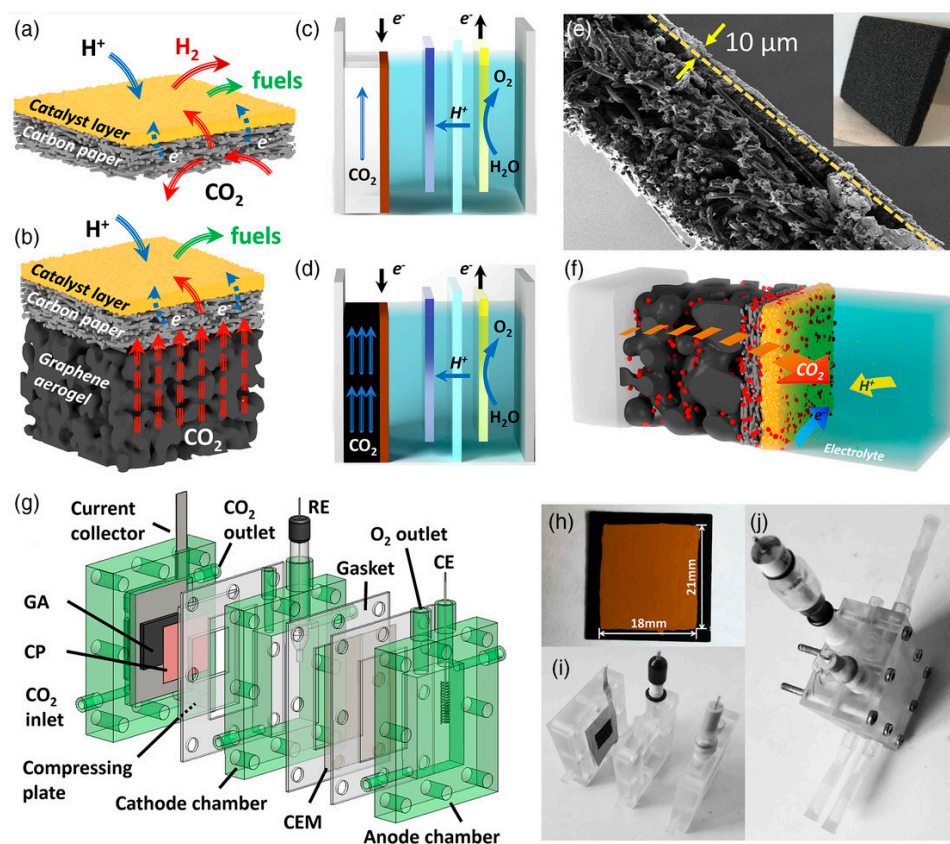

Figure 22. Schematic illustrations of design for GACP-electrode. Reproduced from Ref. [21]. Copyright (2017), with permission from Wiley.

4. Conclusions and Outlook

We summarized the recent research progress in ice-templated materials (ITM) for electrochemical energy storage and conversion, with a focus on their application in supercapacitors, Li-ion batteries, and fuel cells. Although the ice-templating method has yielded promising results, significant challenges remain. These include: (i) the time-consuming and energy-intensive freeze-drying process required to remove ice templates; (ii) the limited scalability of ice-templated materials due to the lowest temperature that restricts ice crystal growth; (iii) the lengthy fabrication periods due to the slow velocity of the ice front; and (iv) the difficulty in controlling ice growth leading to inconsistent sample batches. To address these issues, in situ observation of ice growth and a comprehensive understanding of the interaction between the ice front and the building blocks are necessary.

In recent years, there have been numerous research endeavors aimed at expanding the capabilities of ice-templating methods. One promising development is the ice-dissolving–complexation process, which operates at room temperature and can replace freeze-drying for obtaining ice-templated materials. Efforts have also focused on the assembly and movement of colloidal particles during freezing to provide guidance for the ice-templating process. The utilization of ITM technologies will be crucial for the development of prototypes in energy storage, particularly in enhancing battery mass/ion/charge transfer capabilities to improve battery capacity and reaction efficiency. Therefore, a more comprehensive understanding of freezing mechanisms and their integration with other techniques has the potential to fabricate novel materials with exceptional properties. These materials hold tremendous potential for electrochemical engineering applications, such as supercapacitors, Li-ion batteries, and fuel cells. Further exploration, innovation, and implementation initiatives aimed at lowering costs from their present levels would result in decreased energy system costs associated with decarbonization, and it would facilitate the global shift towards cleaner, low-carbon energy sources.

References

1. Kannan, N.; Vakeesan, D. Solar energy for future world: A review. *Renew. Sustain. Energy Rev.* **2016**, *62*, 1092–1105. [CrossRef]
2. Herbert, G.J.; Iniyan, S.; Sreevalsan, E.; Rajapandian, S. A review of wind energy technologies. *Renew. Sustain. Energy Rev.* **2007**, *11*, 1117–1145. [CrossRef]
3. He, X.; Zhang, X. A comprehensive review of supercapacitors: Properties, electrodes, electrolytes and thermal management systems based on phase change materials. *J. Energy Storage* **2022**, *56*, 106023. [CrossRef]
4. Li, L.; Lu, S.; Dai, Y.; Li, H.; Wang, X.; Zhang, Y. Controlled Synthesis of Hierarchical Nanostructured Metal Ferrite Microspheres for Enhanced Electrocatalytic Oxygen Evolution Reaction. *ACS Appl. Nano Mater.* **2023**, *6*, 2184–2192. [CrossRef]
5. Şahin, A.D. Progress and recent trends in wind energy. *Prog. Energy Combust. Sci.* **2004**, *30*, 501–543. [CrossRef]
6. Lu, S.; Hummel, M.; Gu, Z.; Gu, Y.; Cen, Z.; Wei, L.; Zhou, Y.; Zhang, C.; Yang, C. Trash to treasure: A novel chemical route to synthesis of NiO/C for hydrogen production. *Int. J. Hydrogen Energy* **2019**, *44*, 16144–16153. [CrossRef]

7. Jia, H.; Lu, S.; Shin, S.H.R.; Sushko, M.L.; Tao, X.; Hummel, M.; Thallapally, P.K.; Liu, J.; Gu, Z. In situ anodic electrodeposition of two-dimensional conductive metal-organic framework@nickel foam for high-performance flexible supercapacitor. *J. Power Sources* **2022**, *526*, 231163. [CrossRef]

8. Lu, S.; Wang, Y.; Xiang, H.; Lei, H.; Xu, B.B.; Xing, L.; Yu, E.H.; Liu, T.X. Mass transfer effect to electrochemical reduction of CO_2: Electrode, electrocatalyst and electrolyte. *J. Energy Storage* **2022**, *52*, 104764. [CrossRef]

9. Wang, H.; Zheng, X.; Fang, L.; Lu, S. Urea Electrooxidation in Alkaline Environment: Fundamentals and Applications. *ChemElectroChem* **2023**, e202300138. [CrossRef]

10. Shao, Y.; El-Kady, M.F.; Sun, J.; Li, Y.; Zhang, Q.; Zhu, M.; Wang, H.; Dunn, B.; Kaner, R.B. Design and mechanisms of asymmetric supercapacitors. *Chem. Rev.* **2018**, *118*, 9233–9280. [CrossRef]

11. Yan, C.; Han, E.; Yang, X.; Hu, K.; Xu, H.; Li, Y.; He, Y.; Lu, S. Engineering sulfur vacancies on Mo-doped nickel sulfide for enhanced electrochemical energy storage. *Ceram. Int.* **2023**, *49*, 14155–14165. [CrossRef]

12. Yan, C.; Yang, X.; Lu, S.; Han, E.; Chen, G.; Zhang, Z.; Zhang, H.; He, Y. Hydrothermal synthesis of vanadium doped nickel sulfide nanoflower for high-performance supercapacitor. *J. Alloys Compd.* **2022**, *928*, 167189. [CrossRef]

13. Eriksson, E.; Gray, E.M. Optimization and integration of hybrid renewable energy hydrogen fuel cell energy systems—A critical review. *Appl. Energy* **2017**, *202*, 348–364. [CrossRef]

14. Nie, M.; Zhang, L.; Jiang, C.; Tian, X.; Li, Q.; Liu, X.; Du, S.; Lu, S.; Lei, D.; Wang, X. New energy and new power–the prospect of increasing use of polymers in fuel cells. *Plast. Rubber Compos.* **2016**, *45*, 31–42. [CrossRef]

15. Yan, C.; Shen, Y.; Lu, S.; Yuan, J.; Li, Y.; Yang, X.; Han, E.; He, Y. Surfactant-Assisted rGO-PbO₂ Electrode to Boost Acrylamide Degradation in Industrial Sewage. *Ind. Eng. Chem. Res.* **2023**. [CrossRef]

16. Lu, S.; Hummel, M.; Gu, Z.; Wang, Y.; Wang, K.; Pathak, R.; Zhou, Y.; Jia, H.; Qi, X.; Zhao, X. Highly efficient urea oxidation via nesting nano-nickel oxide in eggshell membrane-derived carbon. *ACS Sustain. Chem. Eng.* **2021**, *9*, 1703–1713. [CrossRef]

17. Xue, F.; Kang, S.; Dai, Y.; Li, T.; Shen, P.K.; Zhu, J.; Lu, S.; Fu, X.; Wang, L.; Feng, S. Hierarchical lead grid for highly stable oxygen evolution in acidic water at high temperature. *J. Power Sources* **2021**, *493*, 229635. [CrossRef]

18. Zheng, X.; Zhang, L.; He, W.; Li, L.; Lu, S. Heteroatom-Doped Nickel Sulfide for Efficient Electrochemical Oxygen Evolution Reaction. *Energies* **2023**, *16*, 881. [CrossRef]

19. He, X.; Ling, Z.; Peng, X.; Yang, X.; Ma, L.; Lu, S. Facile synthesis of Cu2SnS3 nanocrystals for efficient nitrogen reduction reaction. *Electrochem. Commun.* **2023**, *148*, 107441. [CrossRef]

20. Fang, L.; Wang, S.; Song, C.; Lu, S.; Yang, X.; Qi, X.; Liu, H. Boosting nitrate electroreduction to ammonia via in situ generated stacking faults in oxide-derived copper. *Chem. Eng. J.* **2022**, *446*, 137341. [CrossRef]

21. Wang, Y.; Lei, H.; Xiang, H.; Fu, Y.; Xu, C.; Jiang, Y.; Xu, B.B.; Yu, E.H.; Gao, C.; Liu, T.X. Porous Bilayer Electrode-Guided Gas Diffusion for Enhanced CO_2 Electrochemical Reduction. *Adv. Energy Sustain. Res.* **2021**, *2*, 2100083. [CrossRef]

22. Sun, H.; Zhu, J.; Baumann, D.; Peng, L.; Xu, Y.; Shakir, I.; Huang, Y.; Duan, X. Hierarchical 3D electrodes for electrochemical energy storage. *Nat. Rev. Mater.* **2019**, *4*, 45–60. [CrossRef]

23. Deville, S. Ice-templating, freeze casting: Beyond materials processing. *J. Mater. Res.* **2013**, *28*, 2202–2219.

24. Lai, K.C.; Lee, L.Y.; Hiew, B.Y.Z.; Thangalazhy-Gopakumar, S.; Gan, S. Environmental application of three-dimensional graphene materials as adsorbents for dyes and heavy metals: Review on ice-templating method and adsorption mechanisms. *J. Environ. Sci.* **2019**, *79*, 174–199.

25. Hiew, B.Y.Z.; Lee, L.Y.; Lee, X.J.; Thangalazhy-Gopakumar, S.; Gan, S.; Lim, S.S.; Pan, G.-T.; Yang, T.C.-K.; Chiu, W.S.; Khiew, P.S. Review on synthesis of 3D graphene-based configurations and their adsorption performance for hazardous water pollutants. *Process Saf. Environ. Prot.* **2018**, *116*, 262–286. [CrossRef]

26. Shehzad, K.; Xu, Y.; Gao, C.; Duan, X. Three-dimensional macro-structures of two-dimensional nanomaterials. *Chem. Soc. Rev.* **2016**, *45*, 5541–5588. [CrossRef] [PubMed]

27. Yu, R.; Shi, Y.; Yang, D.; Liu, Y.; Qu, J.; Yu, Z.-Z. Graphene oxide/chitosan aerogel microspheres with honeycomb-cobweb and radially oriented microchannel structures for broad-spectrum and rapid adsorption of water contaminants. *ACS Appl. Mater. Interfaces* **2017**, *9*, 21809–21819. [PubMed]

28. Thomas, B.; Geng, S.; Wei, J.; Lycksam, H.; Sain, M.; Oksman, K. Ice-Templating of Lignin and Cellulose Nanofiber-Based Carbon Aerogels: Implications for Energy Storage Applications. *ACS Appl. Nano Mater.* **2022**, *5*, 7954–7966. [CrossRef]

29. White, M.A.; Conrad, J.; Ellis, S.N.; Chen, R. Investigations of ice-structuring agents in ice-templated ceramics. *J. Am. Ceram. Soc.* **2017**, *100*, 5066–5074.

30. Yang, Q.; Liu, Q.; Ling, W.; Dai, H.; Chen, H.; Liu, J.; Qiu, Y.; Zhong, L. Porous Electrode Materials for Zn-Ion Batteries: From Fabrication and Electrochemical Application. *Batteries* **2022**, *8*, 223.

31. Judez, X.; Zhang, H.; Li, C.; Eshetu, G.G.; Zhang, Y.; González-Marcos, J.A.; Armand, M.; Rodriguez-Martinez, L.M. Polymer-rich composite electrolytes for all-solid-state Li–S cells. *J. Phys. Chem. Lett.* **2017**, *8*, 3473–3477. [CrossRef] [PubMed]

32. Han, Z.; Li, S.; Xiong, R.; Jiang, Z.; Sun, M.; Hu, W.; Peng, L.; He, R.; Zhou, H.; Yu, C. Low Tortuosity and Reinforced Concrete Type Ultra-Thick Electrode for Practical Lithium–Sulfur Batteries. *Adv. Funct. Mater.* **2022**, *32*, 2108669. [CrossRef]

33. Hu, C.; Zhang, X.; Liu, B.; Chen, S.; Liu, X.; Liu, Y.; Liu, J.; Chen, J. Orderly and highly dense polyaniline nanorod arrays fenced on carbon nanofibers for all-solid-state flexible electrochemical energy storage. *Electrochim. Acta* **2020**, *338*, 135846. [CrossRef]

34. Qie, L.; Chen, W.M.; Wang, Z.H.; Shao, Q.G.; Li, X.; Yuan, L.X.; Hu, X.L.; Zhang, W.X.; Huang, Y.H. Nitrogen-doped porous carbon nanofiber webs as anodes for lithium ion batteries with a superhigh capacity and rate capability. *Adv. Mater.* **2012**, *24*, 2047–2050. [CrossRef] [PubMed]

35. Wu, H.; Xu, N.; Jiang, Z.; Zheng, A.; Shi, Q.; Lv, R.; Ni, L.; Diao, G.; Chen, M. Space and interface confinement effect of necklace-box structural FeS_2/WS_2 carbon nanofibers to enhance Na+ storage performance and electrochemical kinetics. *Chem. Eng. J.* **2022**, *427*, 131002. [CrossRef]

36. Wang, Y.; Kong, D.; Shi, W.; Liu, B.; Sim, G.J.; Ge, Q.; Yang, H.Y. Ice templated free-standing hierarchically WS_2/CNT-rGO aerogel for high-performance rechargeable lithium and sodium ion batteries. *Adv. Energy Mater.* **2016**, *6*, 1601057. [CrossRef]

37. Yu, X.; Pei, C.; Feng, L. Surface modulated hierarchical graphene film via sulfur and phosphorus dual-doping for high performance flexible supercapacitors. *Chin. Chem. Lett.* **2019**, *30*, 1121–1125. [CrossRef]

38. Dong, X.; Xu, C.; Lu, S.; Wang, R.; Shi, Z.; Cui, Q.; You, T. ZIF-8 coupling with reduced graphene oxide to enhance the electrochemical sensing of dopamine. *J. Electrochem. Soc.* **2021**, *168*, 116517. [CrossRef]

39. Lu, S.; Hummel, M.; Chen, K.; Zhou, Y.; Kang, S.; Gu, Z. Synthesis of Au@ ZIF-8 nanocomposites for enhanced electrochemical detection of dopamine. *Electrochem. Commun.* **2020**, *114*, 106715. [CrossRef]

40. Nie, M.; Lu, S.; Lei, D.; Yang, C.; Zhao, Z. Rapid synthesis of ZIF-8 nanocrystals for electrochemical detection of dopamine. *J. Electrochem. Soc.* **2017**, *164*, H952. [CrossRef]

41. Chen, W.; Huang, Y.-X.; Li, D.-B.; Yu, H.-Q.; Yan, L. Preparation of a macroporous flexible three dimensional graphene sponge using an ice-template as the anode material for microbial fuel cells. *RSC Adv.* **2014**, *4*, 21619–21624. [CrossRef]

42. Li, S.; Xiong, R.; Han, Z.; He, R.; Li, S.; Zhou, H.; Yu, C.; Cheng, S.; Xie, J. Unveiling low-tortuous effect on electrochemical performance toward ultrathick LiFePO4 electrode with 100 mg cm^{-2} area loading. *J. Power Sources* **2021**, *515*, 230588. [CrossRef]

43. Colard, C.A.; Cave, R.A.; Grossiord, N.; Covington, J.A.; Bon, S.A. Conducting nanocomposite polymer foams from ice-crystal-templated assembly of mixtures of colloids. *Adv. Mater.* **2009**, *21*, 2894–2898. [CrossRef]

44. Joukhdar, H.; Seifert, A.; Jüngst, T.; Groll, J.; Lord, M.S.; Rnjak-Kovacina, J. Ice templating soft matter: Fundamental principles and fabrication approaches to tailor pore structure and morphology and their biomedical applications. *Adv. Mater.* **2021**, *33*, 2100091. [CrossRef] [PubMed]

45. Arabi, N.; Zamanian, A. Effect of cooling rate and gelatin concentration on the microstructural and mechanical properties of ice template gelatin scaffolds. *Biotechnol. Appl. Biochem.* **2013**, *60*, 573–579. [CrossRef]

46. Zhou, J.; Wang, B. Emerging crystalline porous materials as a multifunctional platform for electrochemical energy storage. *Chem. Soc. Rev.* **2017**, *46*, 6927–6945. [CrossRef] [PubMed]

47. He, W.; Chen, K.; Pathak, R.; Hummel, M.; Reza, K.M.; Ghimire, N.; Pokharel, J.; Lu, S.; Gu, Z.; Qiao, Q. High-mass-loading Sn-based anode boosted by pseudocapacitance for long-life sodium-ion batteries. *Chem. Eng. J.* **2021**, *414*, 128638. [CrossRef]

48. Adhamash, E.; Pathak, R.; Chen, K.; Rahman, M.T.; El-Magrous, A.; Gu, Z.; Lu, S.; Qiao, Q.; Zhou, Y. High-energy plasma activation of renewable carbon for enhanced capacitive performance of supercapacitor electrode. *Electrochim. Acta* **2020**, *362*, 137148. [CrossRef]

49. Nie, M.; Lu, S.; Li, Q.; Liu, X.; Du, S. Facile solvothermal synthesis of HKUST-1 as electrocatalyst for hydrogen evolution reaction. *Sci. Sin. Chim.* **2016**, *46*, 357–364.

50. Wang, Y.; Lei, H.; Lu, S.; Yang, Z.; Xu, B.B.; Xing, L.; Liu, T.X. Cu2O nano-flowers/graphene enabled scaffolding structure catalyst layer for enhanced CO_2 electrochemical reduction. *Appl. Catal. B Environ.* **2022**, *305*, 121022. [CrossRef]

51. Nie, Y.; Qi, X.; Wu, R.; Yang, R.; Wang, H.; Deng, M.; Zhang, S.; Lu, S.; Gu, Z.; Liu, X. Structurally ordered PtFe intermetallic nanocatalysts toward efficient electrocatalysis of methanol oxidation. *Appl. Surf. Sci.* **2021**, *569*, 151004. [CrossRef]

52. Nie, M.; Du, S.; Li, Q.; Hummel, M.; Gu, Z.; Lu, S. Tungsten carbide as supports for trimetallic AuPdPt electrocatalysts for methanol oxidation. *J. Electrochem. Soc.* **2020**, *167*, 044510. [CrossRef]

53. González, A.; Goikolea, E.; Barrena, J.A.; Mysyk, R. Review on supercapacitors: Technologies and materials. *Renew. Sustain. Energy Rev.* **2016**, *58*, 1189–1206. [CrossRef]

54. Xu, X.; Zhou, J.; Nagaraju, D.H.; Jiang, L.; Marinov, V.R.; Lubineau, G.; Alshareef, H.N.; Oh, M. Flexible, highly graphitized carbon aerogels based on bacterial cellulose/lignin: Catalyst-free synthesis and its application in energy storage devices. *Adv. Funct. Mater.* **2015**, *25*, 3193–3202. [CrossRef]

55. Zhang, Y.; Zhao, C.; Ong, W.K.; Lu, X. Ultrafast-freezing-assisted mild preparation of biomass-derived, hierarchically porous, activated carbon aerogels for high-performance supercapacitors. *ACS Sustain. Chem. Eng.* **2018**, *7*, 403–411. [CrossRef]

56. Geim, A.K. Graphene: Status and prospects. *Science* **2009**, *324*, 1530–1534. [CrossRef]

57. Ni, Y.; Qi, J.; Zhou, B.; Zhu, L.; Ren, Y.; Zhang, D. Controllable synthesis of multilayered porous carbon by ice templating with graphene addition for supercapacitors. *J. Mater. Sci.* **2021**, *56*, 7533–7546. [CrossRef]

58. Mochizuki, D.; Tanaka, R.; Makino, S.; Ayato, Y.; Sugimoto, W. Vertically aligned reduced graphite oxide nanosheet film and its application in a high-speed charge/discharge electrochemical capacitor. *ACS Appl. Energy Mater.* **2019**, *2*, 1033–1039. [CrossRef]

59. Dey, R.S.; Hjuler, H.A.; Chi, Q. Approaching the theoretical capacitance of graphene through copper foam integrated three-dimensional graphene networks. *J. Mater. Chem. A* **2015**, *3*, 6324–6329. [CrossRef]

60. Kota, M.; Yu, X.; Yeon, S.-H.; Cheong, H.-W.; Park, H.S. Ice-templated three dimensional nitrogen doped graphene for enhanced supercapacitor performance. *J. Power Sources* **2016**, *303*, 372–378. [CrossRef]

61. Guo, S.; Kang, S.; Feng, S.; Lu, W. MXene-enhanced deep ultraviolet photovoltaic performances of crossed Zn2GeO4 nanowires. *J. Phys. Chem. C* **2020**, *124*, 4764–4771. [CrossRef]

62. Zhao, M.Q.; Xie, X.; Ren, C.E.; Makaryan, T.; Anasori, B.; Wang, G.; Gogotsi, Y. Hollow MXene spheres and 3D macroporous MXene frameworks for Na-ion storage. *Adv. Mater.* **2017**, *29*, 1702410. [CrossRef] [PubMed]

63. Gao, G.; Yang, S.; Wang, S.; Li, L. Construction of 3D porous MXene supercapacitor electrode through a dual-step freezing strategy. *Scr. Mater.* **2022**, *213*, 114605. [CrossRef]

64. Cai, C.; Wei, Z.; Deng, L.; Fu, Y. Temperature-invariant superelastic multifunctional MXene aerogels for high-performance photoresponsive supercapacitors and wearable strain sensors. *ACS Appl. Mater. Interfaces* **2021**, *13*, 54170–54184. [CrossRef]

65. Zhang, P.; Zhu, Q.; Soomro, R.A.; He, S.; Sun, N.; Qiao, N.; Xu, B. In situ ice template approach to fabricate 3D flexible MXene film-based electrode for high performance supercapacitors. *Adv. Funct. Mater.* **2020**, *30*, 2000922. [CrossRef]

66. Xia, Z.; Sun, R.; Jing, F.; Wang, S.; Sun, H.; Sun, G. Modeling and optimization of Scaffold-like macroporous electrodes for highly efficient direct methanol fuel cells. *Appl. Energy* **2018**, *221*, 239–248. [CrossRef]

67. Zhao, Y.; Alsaid, Y.; Yao, B.; Zhang, Y.; Zhang, B.; Bhuskute, N.; Wu, S.; He, X. Wood-inspired morphologically tunable aligned hydrogel for high-performance flexible all-solid-state supercapacitors. *Adv. Funct. Mater.* **2020**, *30*, 1909133. [CrossRef]

68. Wei, J.; Yin, C.; Wang, H.; Wang, Q. Polyampholyte-doped aligned polymer hydrogels as anisotropic electrolytes for ultrahigh-capacity supercapacitors. *J. Mater. Chem. A* **2018**, *6*, 58–64. [CrossRef]

69. Liu, X.; Taiwo, O.O.; Yin, C.; Ouyang, M.; Chowdhury, R.; Wang, B.; Wang, H.; Wu, B.; Brandon, N.P.; Wang, Q. Aligned ionogel electrolytes for high-temperature supercapacitors. *Adv. Sci.* **2019**, *6*, 1801337. [CrossRef]

70. Kim, S.W.; Seo, D.H.; Ma, X.; Ceder, G.; Kang, K. Electrode materials for rechargeable sodium-ion batteries: Potential alternatives to current lithium-ion batteries. *Adv. Energy Mater.* **2012**, *2*, 710–721. [CrossRef]

71. Zhao, Z.; Sun, M.; Chen, W.; Liu, Y.; Zhang, L.; Dongfang, N.; Ruan, Y.; Zhang, J.; Wang, P.; Dong, L. Sandwich, vertical-channeled thick electrodes with high rate and cycle performance. *Adv. Funct. Mater.* **2019**, *29*, 1809196. [CrossRef]

72. Huang, C.; Dontigny, M.; Zaghib, K.; Grant, P.S. Low-tortuosity and graded lithium ion battery cathodes by ice templating. *J. Mater. Chem. A* **2019**, *7*, 21421–21431. [CrossRef]

73. Roberts, A.D.; Wang, S.; Li, X.; Zhang, H. Hierarchical porous nitrogen-rich carbon monoliths via ice-templating: High capacity and high-rate performance as lithium-ion battery anode materials. *J. Mater. Chem. A* **2014**, *2*, 17787–17796. [CrossRef]

74. Zhai, H.; Xu, P.; Ning, M.; Cheng, Q.; Mandal, J.; Yang, Y. A flexible solid composite electrolyte with vertically aligned and connected ion-conducting nanoparticles for lithium batteries. *Nano Lett.* **2017**, *17*, 3182–3187. [CrossRef] [PubMed]

75. Lei, H.; Xing, L.; Jiang, H.; Wang, Y.; Xu, B.B.; Xuan, J.; Liu, T.X. Designing graded fuel cell electrodes for proton exchange membrane (PEM) fuel cells with recurrent neural network (RNN) approaches. *Chem. Eng. Sci.* **2023**, *267*, 118350. [CrossRef]